Astron. Astrophys. 333, 1069–1081 (1998)

ASTRONOMY
AND
ASTROPHYSICS

Hydrogen and helium in the solar chromosphere: a background model for fractionation

Hardi Peter[⋆] **and Eckart Marsch**

Max-Planck-Institut für Aeronomie, D-37189 Katlenburg-Lindau, Germany (hpeter@linmpi.mpg.de)

Received 11 August 1997 / Accepted 3 February 1998

Abstract. A multi-fluid model for a hydrogen-helium mixture in an ionization-diffusion layer in the (solar) chromosphere is presented. The purpose of this model is to serve as a background for fractionation models calculating the abundance variations of minor species from the photosphere to the solar wind. The emphasis will be on the determination of the (mean) flow velocity in that ionization layer. The equations of continuity and momentum of every component, neutral and (singly) ionized for both elements, will be solved together with an energy equation including heating and radiative losses. Special attention will be paid to the ionization and the elastic collisions as well as to resonant charge exchange. One of the main results is the connection of the particle flux through the chromosphere with the ionization rate, i.e. with the photon flux in the UV. Furthermore the abundance variations of helium are discussed with the result, that the ion-neutral separation processes leading to the fractionation of the minor elements cannot explain the fractionation of helium as measured in the solar wind.

Key words: Sun: chromosphere – Sun: abundances – solar wind

1. Introduction

The elemental abundances vary from the photosphere of the sun to the interplanetary space. A comparison of spectroscopic observations in the photosphere with in-situ measurements in the solar wind or spectroscopic observations in the corona clearly show, that elements with a first ionization potential (FIP) below 10 eV are enriched in relation to those with higher FIP. The factor of enhancement varies from 2 (fast wind) over 4 (slow wind) up to 10 (polar plumes) depending on the respectively observed structure. See Anders & Grevesse (1989), von Steiger et al. (1995), Hénoux & Somov (1992), Hénoux (1995) and Meyer (1996) for collections of the measurements and a review of different attempts to describe this so-called FIP-effect theoretically.

It is now widely accepted that the basic mechanism for fractionation of elements is driven by an ion-neutral separation in the chromosphere, well above the temperature minimum and near but below 10^4 K (Geiss 1982). For this the recent fractionation models, which allowed for the first time a detailed quantitative comparison with the measurements, assumed the trace gases to diffuse on a background of hydrogen and to be ionized by the UV-photons coming from the higher layers of the chromosphere and transition region: von Steiger & Geiss (1989) and Marsch et al. (1995) were able to explain the fractionation in the slow wind, while recently Peter (1996) found a velocity-dependence of the fractionation, which leads to the understanding of the FIP-effect in the slow *and* the fast wind within the same model.

For a more advanced fractionation model, capable of explaining also other phenomena like the strong enrichments of magnesium in polar plumes (observations e.g. of Widing & Feldman 1992) or the "absolute" fractionation, i.e. the fractionation in relation to hydrogen (measurements of von Steiger et al. 1995), a sophisticated model for the main gas, i.e. the background, is needed. This paper offers just such a model.

The aim is to define the background for a fractionation model, which can describe the abundance variation from the photosphere to the solar wind or corona. There are two major constraints for such a main gas model: on the one hand the flow of the material has to be treated self-consistently, because the fractionation connects the abundances on solar surface with those in the solar wind. Since the fractionation processes are located in the chromosphere one has to describe the source region of the solar wind including the plasma flow.

On the other hand such a main gas model has to be also the model atmosphere for the chromosphere. In the last two decades many comprehensive atmospheric models were published, e.g. the continuum atmosphere by Gingerich & de Jager (1968), the semi-empirical model of Vernazza et al. (1981) or the one of Fontenla et al. (1990) including ambipolar diffusion. But all these models assume a static atmosphere and do not include a self-consistent treatment of the flow.

Of course, a complete model combining the source region of the solar wind with the upper atmospheric layers, would be the ultimate goal. Yet, it is very complicated to combine an exact treatment of the radiative transport with the plasma dynamics and thermodynamics, and therefore one has to simplify the problem. Because the aim of this paper is to offer a main gas model for the description of a solar-wind-related phenomenon,

Send offprint requests to: Hardi Peter

⋆ *Present address:* High Altitude Observatory/NCAR, P.O. Box 3000, Boulder, CO 80307-3000, USA

the main emphasis will be on the flows. Radiative transport will not be included, but special attention will be paid on the ionization of the material. Thus the present model *is not* a full atmospheric model for the chromosphere, but it may serve well as a background for the minor ion fractionation.

Another aim of this paper is to elucidate the special role of helium: its abundance, which is about 10% in the photosphere, varies from some percent in the "quiet" solar wind (Schwenn 1990) to up to 40% in the driver gas of flare-induced interplanetary shocks (Hirschberg et al. 1970, Borrini et al. 1982). With an abundance of 10% and an atomic weight four times higher than hydrogen, helium contributes about one fourth to the total mass and can thus not be treated as a trace gas, i.e. as test particles, but must be included in the main gas, with collisional coupling to the hydrogen. As it turns out, the wide variations of the helium abundances cannot be understood on the basis of an ionization-diffusion model for a thin layer in the chromosphere.

The models presented in this paper are an extension of the main gas model of Marsch et al. (1995), who only considered diffusion and (photo-) ionization. In the present models also the effects of e.g. the absorption of the ionizing radiation, the recombination and the gravitation are considered. This will remove the problems of their simple main gas model, like the infinite proton speed at the bottom. Additionally an energy equation is solved to determine the temperature structure. This makes possible to study the influence of the flows on the temperature profile.

In the next section at first the assumed geometry and the basic assumptions as used in the model are presented, before in Sect. 3 the model equations are established. This section also describes the ionization and elastic collisions as well as heating, radiative cooling and heat flux. Before discussing the results for a pure hydrogen gas in Sect. 5 an analytical approximation for this case will be presented in Sect. 4. At least the effects of helium will be considered in Sect. 6 and the resulting abundance variations will be discussed. Sect. 7 summarizes the results of the paper.

2. Geometry and assumptions

As is suggested e.g. by Hα-filtergrams, the chromosphere is a highly structured region, and it is highly variable on long timescales of some days (e.g. chromospheric network) as well as on short timescales of minutes and seconds (e.g. spicules or bright points). Thus the first conclusion would be that a stationary description of the atmosphere is impossible.

Nevertheless, stationary and steady models, like those of Vernazza et al. (1981), contributed a lot to the understanding of the relevant processes in the atmosphere. Even if the chromosphere is in a highly non-stationary state, a stationary model should give us a basic idea of the relevant processes by describing a "mean chromosphere", which probably does not exist in the real solar atmosphere. This philosophy corresponds with the one of climate models: without resolving the weather, these can describe some of the basic mechanisms leading to the global behaviour of e.g. the temperature runs in the earth's atmosphere.

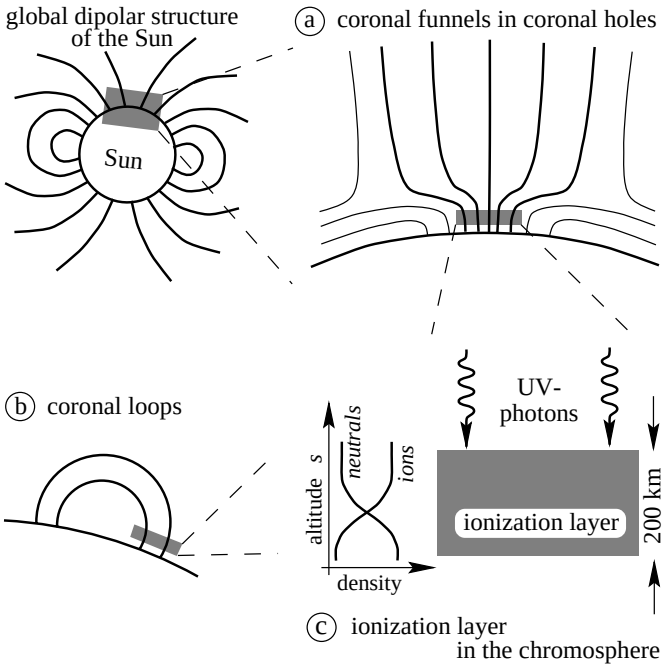

Fig. 1a–d. Sketch of the geometry in the source regions of the fast and slow wind. (see text).

As the main aim of this paper is to study in detail the source region of the solar wind, the application of a *stationary* model is suggested also by recent ULYSSES results: Barnes et al. (1995) found, that the particle flux density in the fast solar wind (normalized to 1 AU) is nearly constant, regardless of heliocentric longitude, latitude and distance or time in the solar cycle. Thus if the interest is in a *mean* behaviour, it is justified, given the steadiness of the fast wind, to apply stationary conditions also in the chromosphere.

2.1. Geometry

Concerning the geometry of the source regions of the solar wind, for the fast and the slow wind the following two pictures may be applicable (see Fig. 1).

1. Fast solar wind

Between the super-granulation cells vertical magnetic field emerges, which widens up to form the so called canopy and build up the coronal funnels (Dowdy 1986; Fig. 1a). A possible scenario is that the fast wind leaves the sun through these funnels. At the bottom of the funnels, in the chromosphere, the magnetic field is vertical and a one-dimensional stratification is a good approximation (see Fig. 1c)

The velocity in the bottom region of the funnel can be calculated in the following way: At the earth's orbit, at 1 AU, the particle flux density in the high speed wind is $\Phi_{1\,\mathrm{AU}} \approx 2{\cdot}10^{12}\,\mathrm{m^{-2}s^{-1}}$ (Schwenn 1990). Mapping this flux back to the chromosphere, by using the geometry factors of the spherical expansion from $1\,R_\odot$ to $1\,\mathrm{AU} \approx 215\,R_\odot$ ($1/215^2$), the

over-spherical expansion in the fast wind (1/7 after Kopp & Holzer 1976) and the partial filling of the solar surface by coronal funnels ($\approx$ 2% after Athay 1981), leads to a particle flux at the bottom of the funnels, i.e. in the chromosphere, of $\Phi_{\rm chromo} \approx 3{\cdot}10^{19}\,{\rm m^{-2}s^{-1}}$. Using the density of $8{\cdot}10^{16}\,{\rm m^{-3}}$ at 8000 K from the atmosphere model of Vernazza et al. (1981), this flux leads to a velocity of the order of $U \approx 500$ m/s.

2. Slow solar wind

In this case the situation is much more complicated. But one possible scenario may be the following: at the top of large coronal loops material is accumulated because of a continuous flow into the loop at its footpoints (see Fig. 1b). Thus from time to time the loops in the equatorial streamer belt have to open and let the accumulated material go out into interplanetary space, forming the variable slow wind (see the recent SOHO observations of Sheeley et al. 1997). In the chromospheric lower part of the loop, which is small compared to the whole loop, the conditions are locally comparable to those at the base of the coronal funnels.

Even if these are very simplifying scenarios they do account for the basic geometric properties as known today. In both cases a one-dimensional stratified atmospheric layer can be assumed to exist in the chromosphere, if the interest is in its the mean behaviour as the source region of the solar wind.

2.2. Assumptions

Besides the so far discussed assumptions — time stationarity, homogeneous vertical magnetic field and one-dimensional stratification — some more obvious assumptions are made.

The material in the chromosphere is ionized by the UV radiation coming from higher layers. This radiation is (partly) absorbed in the chromosphere (see Sect. 3.2). This is a strong simplification — normally the full problem of the radiative transport has to be considered. But up to now no models are available which can handle the radiative transport *and* the plasma dynamics self-consistently. As a first step this paper concentrates on the latter aspects, an approach which leads to a simplification in the treatment of the radiation.

In the chromosphere the thermal coupling between the different species is still strong enough to equilibrate temperatures. Thus only one energy equation is used to describe the thermodynamics. Additionally, in this energy equation the effects of heating and radiative cooling are simply parameterized as functions of the temperature and density (see Sect. 3.3).

Finally it should be stated that the plasma is assumed to be quasi-neutral and bear no net current.

3. Model equations

For the description of the transport in plasma a (stationary) five-moment-approximation of Boltzmann's equation will be used (see e.g. Schunk, 1975). In the energy balance heating and radiative cooling are included as parameterized functions of temperature and density. The moment expansion is closed by assuming the pressure (of an ideal gas) to be isotropic, $p = n\,k_{\rm B}\,T$, and that the classical formulation of the heat flux proportional to the temperature gradient can be used (Sect. 3.3). In Sect. 3.4 and 3.5 numerical solutions of the equations are described and the boundary conditions are formulated.

3.1. Multi-fluid transport equations

In the formulation of Marsch et al. (1995) the stationary *equations of continuity and momentum* for a species j read as

$$\nabla \cdot (n_j\,\boldsymbol{u}_j) \;=\; \sum_{j'} \left(\gamma_{j'\,j}\,n_{j'} - \gamma_{jj'}\,n_j\right), \tag{1}$$

$$\begin{aligned}(\boldsymbol{u}_j \cdot \nabla)\boldsymbol{u}_j \;+\; \frac{1}{n_j}\,\nabla(v_j^2\,n_j) \;+\; \frac{Z_j}{n_{\rm e}}\,\nabla(c_j^2\,n_{\rm e}) \;-\; \boldsymbol{g} \;=\\ =\; -\sum_k \nu_{jk}\,(\boldsymbol{u}_j - \boldsymbol{u}_k) \;-\; \sum_{j'} \frac{n_{j'}}{n_j}\gamma_{j'\,j}\,(\boldsymbol{u}_j - \boldsymbol{u}_{j'})\\ +\; \sum_k \omega_{jk}\,(\boldsymbol{u}_j - \boldsymbol{u}_k) \times \hat{\boldsymbol{b}}.\end{aligned} \tag{2}$$

Here n_j and $\boldsymbol{u}_j$ denote the particle density and the velocity of the species j. The sources and sinks for the particle flux density, $n_j\,\boldsymbol{u}_j$, are due to ionization and recombination with the respective rates $\gamma_{j'\,j}$.

In this paper the indices k, j, and j' are used. Whenever k and j are found, an interaction of the the type $j,\ k \leftrightarrow j,\ k$ is present, i.e. the particles stay the same, e.g. as in elastic collisions. j and k represent different elements. j and k are used also in the case of resonant charge exchange, e.g. H, $H^+ \leftrightarrow H^+$, H, because before and after the interaction the same particles are present, just with exchanged identity. In a reactive interaction (e.g. ionization), the particles before and after the interaction are not the same, but they can change their state of excitation or ionization. Because they are from the same element, the same letter is used, with or without a prime: j and j'. In contrast to Marsch et al. (1996) we do not use j and j^+ because j and j' are more general: e.g. the continuity equation (1) is valid for both, neutrals and ions. If we would have used j and j^+, we would have to distinguish between the case of neutrals and ions, because there is no symmetry between the ionization and recombination rate. Additionally j and j' can also be used to describe excitation and de-excitation processes.

The sound speed and the ion-acoustic speed are given by $v_j = (k_{\rm B}T_j/m_j)^{1/2}$ and $c_j = (k_{\rm B}T_{\rm e}/m_j)^{1/2}$ respectively, with Boltzmann's constant $k_{\rm B}$, the temperature T_j and the atomic mass m_j. In the present case of equal temperatures, $T_j = T_{\rm e}$, these two speeds are equal, $c_j = v_j$. Z_j denotes the charge number of the species j and $\boldsymbol{g}$ is the gravitational acceleration.

The exchange of momentum between the species is due to elastic collisions and ionization/recombination with the respective rates ν_{jk} and $\gamma_{j'\,j}$ (see Sect. 3.2). The influence of the magnetic field can be formulated in an analogous way with a "magnetic" frequency $\omega_{jk} = \Omega_j\,Z_k\,n_k/n_{\rm e}$. Here $\Omega_j = Z_j\,e\,B/m_j$

is the gyro-frequency with the elementary charge e and the magnetic field strength B. The direction of the magnetic field is given by $\hat{\boldsymbol{b}} = \boldsymbol{B}/B$. Both the elastic collision frequencies and the "magnetic" frequencies obey the symmetry relations $m_j\, n_j\, \nu_{jk} = m_k\, n_k\, \nu_{kj}$ and $m_j\, n_j\, \omega_{jk} = m_k\, n_k\, \omega_{kj}$.

The term $\propto \gamma_{j'\,j}(u_j - u_{j'})$ in (2) describes the momentum that a particle which is created or destroyed (by ionization/recombination) adds or subtracts to the momentum of the species (see e. g. Geiss & Bürgi 1986). This was neglected in the model of Marsch et al. (1995) because the ionization/recombination rates are some orders of magnitude smaller than the momentum transport due to resonant charge exchange; compare (9) and Table 2 with Table 1. But as it can be seen immediately from (2) this term can become important if the density of either the neutral or the ionized species becomes very low. Thus this term is considered in all numerical solutions.

In the derivation of the momentum equation (2) the mass of the electrons was assumed to be much smaller than the mass of the ions, $m_\mathrm{e} \ll m_j$, and quasi-neutrality and zero-current was presumed,

$$n_\mathrm{e} = \textstyle\sum_j Z_j\, n_j, \quad n_\mathrm{e}\, \boldsymbol{u}_\mathrm{e} = \textstyle\sum_j Z_j\, n_j\, \boldsymbol{u}_j. \tag{3}$$

The (ambipolar) electric field is given by $\boldsymbol{E} = -(\boldsymbol{u}_\mathrm{e} \times \boldsymbol{B}) - \nabla(n_\mathrm{e} k_\mathrm{B} T_\mathrm{e})/(e\, n_\mathrm{e})$, a relation which has been exploited in the derivation of (2).

As outlined in Sect. 2.2 the temperature is assumed to be the same for all species, $T = T_\mathrm{e} = T_j$. For this only one *energy equation* has to be solved. Following Schunk (1975) the energy equation for the electrons is given by

$$(\boldsymbol{u}_\mathrm{e} \cdot \nabla)\left(\frac{3}{2}\, n_\mathrm{e}\, k_\mathrm{B}\, T\right) + \frac{5}{2}\, n_\mathrm{e}\, k_\mathrm{B}\, T\, \nabla \cdot \boldsymbol{u}_\mathrm{e} + \nabla \cdot \boldsymbol{q} \;=\; \mathcal{E}. \tag{4}$$

The sources and sinks in the energy balance are due to

$$\mathcal{E} \;=\; \sum_j \sqrt{2}\, Z_j^2\, \nu_{\mathrm{ee}}\, n_e\, m_j\, (\boldsymbol{u}_j - \boldsymbol{u}_\mathrm{e})^2 \;+\; H \;-\; L, \tag{5}$$

namely elastic collisions with the heavy ions, heating and cooling. Often also the heat flux $\nabla{\cdot}\boldsymbol{q}$ is comprehended as a source or sink of energy. These processes are discussed in more detail in Sect. 3.3.

3.2. Ionization, recombination and collisions

In the chromosphere the material becomes (first) ionized, and thus in the particle dynamics ionization and recombination play an important role. Additionally elastic collisions are of importance, particularly in the nearly neutral regions of the atmosphere where diffusion may be of relevance.

Ionization

In the atmospheric layer considered here the most important process is *photoionization*, for which the rate for hydrogen is about $\gamma_\mathrm{Hp}^{(\mathrm{ph.})} \approx 0.014\,\mathrm{s}^{-1}$ (von Steiger & Geiss 1989). This process overwhelms ionization due to electron collisions at chromospheric temperatures of $10^4\,\mathrm{K}$ by some orders of magnitude: following Lotz (1967) the corresponding rate is $\gamma_\mathrm{Hp}^{(\mathrm{el.})} \approx 7.8{\cdot}10^{-5}\,\mathrm{s}^{-1}$.

With the photoionization rate and the typical diffusion velocity as mentioned in Sect. 2.1 one can define an ionization length

$$l_\mathrm{ion} = U/\gamma_\mathrm{ion}, \tag{6}$$

which is of the order of 50 km. Thus the thickness of the ionization layer of hydrogen is somewhat smaller than the gravitational scale height in the chromosphere (300 km), but not negligibly small.

As in models for the earth's ionosphere (see e. g. Banks & Kockarts, 1973), the chromosphere is assumed to be irradiated from above by UV-photons originating in the transition region and corona. In the considered layer these photons are absorbed in the ionization process. As a consequence, the ionization rate will vary with depth in the atmosphere. The below presented description of this variation of the ionization rate follows the one given in the analytical model of Peter & Marsch (1997). For a further discussion of the assumptions leading to (7) see their paper. The change of the ionizing radiative flux ϕ over the distance $\mathrm{d}s$ is proportional to the flux itself and the density n of the absorbing material: $\mathrm{d}\phi \propto n\phi\,\mathrm{d}s$. If the cross section σ for photoionization is assumed to be nearly constant over the relevant wavelength band, then one can apply the same relation to the ionization rate: if s is the vertical coordinate, the respective photoionization rates of hydrogen and helium are determined by

$$\frac{\mathrm{d}}{\mathrm{d}s}\,\gamma_{ni} \;=\; \overline{\sigma}_n\, \gamma_{ni}\, n_n, \tag{7}$$

where the indices n and i stand for the neutral and ionized components of the respective elements. This corresponds to the processes as found in the earth's ionosphere (see e. g. the textbook of Banks & Kockarts 1973). The latter equation for the ionization rate has to be solved together with the transport equations (1), (2) and (4).

The cross sections for photoionization as needed in the description of the ionization rate (7) are taken from Vernazza et al. (1981). The mean values (see Peter & Marsch 1997) can be estimated as

$$\begin{aligned} &\text{hydrogen:} \quad \overline{\sigma}_\mathrm{H}\,[\mathrm{m}^2] = \; 5.5{\cdot}10^{-22}, \\ &\text{helium:} \quad \overline{\sigma}_\mathrm{He}\,[\mathrm{m}^2] = \; 5.2{\cdot}10^{-22}. \end{aligned} \tag{8}$$

This treatment of the ionization rate and photon flux is just an approximation: on the one hand the cross sections and the photon flux depend on the wavelength, on the other hand the exited states of the hydrogen atom are neglected. Thus in a complete atmospheric model one would have to solve not only two continuity and momentum equations in the case of a pure hydrogen gas, but 26 if e. g. a 12-level hydrogen atom is described (two for every level and two for the protons). Additionally one would have to solve properly the rate equation for the photon flux as a function of wavelength.

Table 1. Collisional rates in a hydrogen-helium mixture consisting of neutral and (first) ionized components. T_4 and $n_{k,16}$ denote the temperature in 10^4 K and the particle density in $10^{16}\,\mathrm{m}^{-3}$ respectively (from Geiss & Bürgi, 1986 and von Steiger & Geiss, 1989).

j	k	collision frequency: $\frac{\nu_{jk}}{n_{k,16}}\ [\mathrm{s}^{-1}]$	dominant interaction
H	p	$118\,T_4^{1/2}\,(1-0.125\log T_4)^2$	RCE
He	H	$3.30\,T_4^{0.3}$	hard spheres
He	p	2.67	induced dipole
He^+	H	4.71	induced dipole
He^+	p	$2500\,T_4^{-3/2}$	Coulomb
He	He^+	$34.4\,T_4^{1/2}\,(1-0.148\log T_4)^2$	RCE
e^-	e^-	$182\,m_\mathrm{p}/m_\mathrm{e}\,T_4^{-3/2}$	Coulomb

This has been done e. g. by Vernazza et al. (1981) or Fontenla et al. (1990). But they solved these equations just for the single-fluid hydrostatic case, i. e. for zero velocities, and thus did not have to solve the momentum equations. In contrast, in the present paper the emphasis is on the diffusion and flow of the material. To avoid the problem of combining the radiative transport with the plasma dynamics we use the practical approach described above, where we consider a "mean" or "effective" hydrogen atom. A more complete model including radiative transport would probably result in a (slightly) different profile of the ionization rate with depth, but this should not change the main results for the plasma dynamics.

Recombination

The respective rates for the recombination are simply taken from von Steiger & Geiss (1989).

$$\begin{aligned}\text{hydrogen:}\quad & \gamma_\mathrm{p,H}\,[10^{-3}\,\mathrm{s}^{-1}] = 4.3\,T_4^{-2/3}\,n_\mathrm{e,16},\\ \text{helium:}\quad & \gamma_\mathrm{He^+,\,He}\,[10^{-3}\,\mathrm{s}^{-1}] = 2.1\,T_4^{-0.672}\,n_\mathrm{e,16}.\end{aligned}\tag{9}$$

Here T_4 denotes the temperature in 10^4 K and $n_{k,16}$ the particle density in $10^{16}\,\mathrm{m}^{-3}$.

Elastic collisions

As this paper deals with a mixture of hydrogen and helium, each being either neutral or (singly) ionized, the following processes in the elastic collisions have to be considered: hard sphere collisions (between neutrals), induced dipole interaction (ions and neutrals) and Coulomb-collisions (ions). The respective collisional rates are derived in various textbooks, e. g. in Burgers (1969). For the collisions between the neutral and ionized particles of hydrogen as well as helium the resonant charge exchange (RCE) is the most important process. The respective cross sections can be found in Banks (1966).

In this paper the (parameterized) collisional rates as given in Geiss & Bürgi (1986) and von Steiger & Geiss (1989) are used. These are listed in Table 1.

3.3. Energy sources and sinks

The energy sources and sinks are of great importance for the energy balance in the lower atmosphere. The most important processes are mechanical heating and radiative losses. The loss of kinetic energy (of the electrons) due to collisional ionization can be neglected in the lower chromosphere, because it is not efficient at those low temperatures. However, in a model which includes the transition region this process would have to be taken into account.

Heating

The exact determination of the heating rate is an unresolved problem. For that reason mostly parameterizations are used.

Following Ulmschneider & Kalkofen (1977) the heating in the lower chromosphere is due to the damping of shocks. Priest (1982) gave some heuristic arguments that in this case the heating rate behaves like $H \propto p/T^{1/2}$ and is exponentially damped. This result corresponds to the behaviour of H as described by Rosner et al. (1978).

With parameter values taken from the references mentioned above, giving a damping length of about 3000 km and an energy flux of $5{\cdot}10^5\,\mathrm{W/m}^2$ at the bottom of the chromosphere, the resulting heating rate is

$$H\,[\mathrm{W/m}^3] = 0.2\,n_\mathrm{p,16}\,T_4^{1/2}\,\exp(-s/3000\,\mathrm{km}).\tag{10}$$

Once more, $n_\mathrm{p,16}$ and T_4 are the density in $10^{16}\,\mathrm{m}^{-3}$ and the temperature in 10^4 K respectively.

Radiative cooling

Besides heat conduction radiative cooling is the most important energy loss process. Although the radiation is emitted by the atoms and ions, this process is a loss mechanism for the energy of the electrons, since the excitation of the atoms and ions is due to electron collisions and thus the required energy is taken from the kinetic energy of the electrons.

If the radiation is not treated self-consistently, an approximate description is required. For this purpose the radiative loss function L is often assumed to be a power law of the temperature. A great variety of work has been done on this subject.

The description in the present paper will follow the work of Peres et al. (1982). For chromospheric temperatures they give the following parameterization:

$$L\,[10^{-5}\,\mathrm{W/m}^3] = n_\mathrm{e,16}\,n_\mathrm{H,16}\,\alpha\,T_4^{\chi},\tag{11}$$

$$\text{with}\quad \begin{cases} \alpha = 7.95, & \chi = 11.7 \quad : \quad 0.44 \le T_4 \le 0.8 \\ \alpha = 1.96, & \chi = 6.15 \quad : \quad 0.8 \le T_4 \le 2 \end{cases}$$

As before, the indices $_{16}$ and $_4$ indicate that the density has to be taken in units of $10^{16}\,\mathrm{m}^{-3}$ and the temperature in 10^4 K.

It should be noted that this treatment is a little problematic, because the main assumption going into (11) is to describe an optically thin plasma. But this may not be true at low temperatures. However, Kuin & Poland (1991) showed that for the

optically thick plasma of a loop a similar (though corrected) radiative loss function can be used.

Heat flux

Instead of describing the heat flux vector by a heat flux moment equation, it is assumed to be proportional to the temperature gradient, i.e.

$$\boldsymbol{q}_\mathrm{e} \;=\; -\kappa_\mathrm{e}\,\nabla T, \tag{12}$$

Following Geiss & Bürgi (1986) this long known relation can be derived by assuming a subsonic flow, an isotropic pressure and time stationarity. In this case the heat flux equation for the electrons can be reduced to

$$\frac{5}{2}\,k_\mathrm{B}\,p_\mathrm{e}\,\nabla T \;=\; -\eta\,m_\mathrm{e}\,\nu_\mathrm{ee}\boldsymbol{q}_\mathrm{e}, \tag{13}$$

with the dimensionless number

$$\eta \;=\; \sum_k\;\frac{13}{10}\,\sqrt{2}\,\frac{n_k}{n_\mathrm{e}} \;+\; \frac{4}{5}. \tag{14}$$

For a plasma consisting only of neutral and singly ionized particles, as considered in the present paper, the quasi-neutrality renders η a constant, $\eta = 1.3\sqrt{2} + 0.8 \approx 2.64$.

Using the value for the collisional rate ν_ee as given in Table 1, the simplified heat flux equation (13) leads directly to the relation (12) with the thermal conductivity along the magnetic field being

$$\kappa_\mathrm{e} \;=\; 0.0593\,T_4^{5/2}\;\;\mathrm{W/(m\,K)}. \tag{15}$$

This relation $\kappa_\mathrm{e} \propto T^{5/2}$ together with (12) is also known as Spitzer's law.

It is just interesting to note that this conductivity in the chromosphere at 10^4 K is of the same order as in the air on the earth at room temperature!

In this paper the conductivity across the magnetic field is not considered, because it is some orders of magnitude smaller than κ_e. Given the strong magnetic fields of $B = 10-100$ Gauß, the electrons are strongly magnetized and despite of collisions constrained to move along field lines.

3.4. Formulation of the transport equations appropriate for numerical treatment

In this section the transport equations (1), (2) and (4) will be formulated for one spatial dimension along the magnetic field (see Sect. 2.1) and in a way appropriate for the numerical treatment. As the aim is to use standard numerical routines solving a system of differential equations of first order, the equations have to be written in the form

$$y_i' = f(y_j, s), \tag{16}$$

where y_i stands for the densities, velocities and temperatures of the respective elements.

Here as in the following the prime, $'$, denotes the derivative with respect to the vertical coordinate s. Concerning the numerical treatment it is better to use the particle flux densities $\phi_j = n_j\,u_j$ instead of the velocities, where u_j is the component of the velocity $\boldsymbol{u}_j$ along the coordinate s. This is because for very low densities the flux remains finite while the velocity can become extremely high due to numerical errors.

First of all the energy equation (4), which is of second order, will be divided into two equations of first order. For this purpose a new variable $q = -\kappa_\mathrm{e}\,T'$, with κ_e from (15), is introduced,

$$T' \;=\; -q/\kappa_\mathrm{e}, \tag{17}$$

$$q' \;=\; \mathcal{E} \;+\; \left(\frac{n_\mathrm{e}'}{n_\mathrm{e}} - \frac{5}{2}\,\frac{\phi_\mathrm{e}'}{\phi_\mathrm{e}}\right)\,\phi_\mathrm{e}\,k_\mathrm{B}\,T \;+\; \frac{3}{2}\,\phi_\mathrm{e}\,k_\mathrm{B}\,\frac{q}{\kappa_\mathrm{e}}. \tag{18}$$

Because n_e' and ϕ_e' can be written in terms of the variables but not their derivatives (see below), the energy equations thus attain the required form (16).

Before re-formulating the continuity and momentum equations the following abbreviations are introduced:

$$\begin{aligned}
\mathcal{N}_j \;&=\; \sum_{j'}(\gamma_{j'j}\,n_{j'} - \gamma_{jj'}\,n_j),\\
\mathcal{M}_j \;&=\; \sum_k\,\frac{\nu_{jk}}{n_k}(\phi_k\,n_j - \phi_j\,n_k) + \sum_{j'}\,\frac{\gamma_{jj'}}{n_j}(\phi_{j'}\,n_j - \phi_j\,n_{j'}),\\
\mathcal{Q}_j \;&=\; \mathcal{M}_j \;-\; \left[g + (1+Z_j)\,(v_j^2)'\right]\,n_j \;-\; (\phi_j/n_j)\,\mathcal{N}_j,\\
\mathcal{R}_j \;&=\; Z_j\,v_j^2\,\frac{n_j}{n_\mathrm{e}},\\
\mathcal{S}_j \;&=\; v_j^2 - (\phi_j/n_j)^2.
\end{aligned}$$

The derivative of the squared sound speed is given by $(v_j^2)' = k_\mathrm{B}T'/m_j \;=\; -(k_\mathrm{B}\,q)/(m_j\,\kappa_\mathrm{e})$. All these abbreviations are functions of the variables itself but not of their derivatives!

Now the equations of continuity and momentum can be written in compact form as

$$\phi_j' \;=\; \mathcal{N}_j, \tag{19}$$

$$n_j' \;=\; \frac{\mathcal{Q}_j}{\mathcal{S}_j} - \frac{\mathcal{R}_j}{\mathcal{S}_j}\,n_\mathrm{e}'. \tag{20}$$

Because of the quasi-neutrality condition (3) this system of equations can always be written in the standard form (16).

In the case of a pure hydrogen plasma the system (19) and (20) reads

$$\begin{aligned}
\phi_\mathrm{H}' \;&=\; \mathcal{N}_\mathrm{H}, \qquad & \phi_\mathrm{p}' \;&=\; -\mathcal{N}_\mathrm{H},\\
n_\mathrm{H}' \;&=\; \mathcal{Q}_\mathrm{H}/\mathcal{S}_\mathrm{H}, \qquad & n_\mathrm{p}' \;&=\; \mathcal{Q}_\mathrm{p}/(\mathcal{S}_\mathrm{p} + \mathcal{R}_\mathrm{p}).
\end{aligned} \tag{21}$$

It is straight forward to obtain the system for the hydrogen-helium mixture. The corresponding eight equations are just a little longer.

$$\begin{aligned}
\phi_\mathrm{H}' &= \mathcal{N}_\mathrm{H}, & \phi_\mathrm{p}' &= -\mathcal{N}_\mathrm{H},\\
n_\mathrm{H}' &= \frac{\mathcal{Q}_\mathrm{H}}{\mathcal{S}_\mathrm{H}}, & n_\mathrm{p}' &= \frac{\mathcal{Q}_\mathrm{p}(\mathcal{S}_{\mathrm{He}^+} + \mathcal{R}_{\mathrm{He}^+}) - \mathcal{Q}_{\mathrm{He}^+}\mathcal{R}_\mathrm{p}}{\mathcal{S}_\mathrm{p}\mathcal{S}_{\mathrm{He}^+} + \mathcal{S}_{\mathrm{He}^+}\mathcal{R}_\mathrm{p} + \mathcal{S}_\mathrm{p}\mathcal{R}_{\mathrm{He}^+}},\\
\phi_\mathrm{He}' &= \mathcal{N}_\mathrm{He}, & \phi_{\mathrm{He}^+}' &= -\mathcal{N}_\mathrm{He},\\
n_\mathrm{He}' &= \frac{\mathcal{Q}_\mathrm{He}}{\mathcal{S}_\mathrm{He}}, & n_{\mathrm{He}^+}' &= \frac{\mathcal{Q}_{\mathrm{He}^+}(\mathcal{S}_\mathrm{p} + \mathcal{R}_\mathrm{p}) - \mathcal{Q}_\mathrm{p}\mathcal{R}_{\mathrm{He}^+}}{\mathcal{S}_\mathrm{p}\mathcal{S}_{\mathrm{He}^+} + \mathcal{S}_{\mathrm{He}^+}\mathcal{R}_\mathrm{p} + \mathcal{S}_\mathrm{p}\mathcal{R}_{\mathrm{He}^+}}.
\end{aligned} \tag{22}$$

It is easily proven, that for vanishing helium components, i.e. the densities and fluxes of He and He^+ are set to zero, this system results in the system (21) for a pure hydrogen gas.

It should be noted that in both systems, in (21) and (22), no use was made of the conservation of flux. It would have been easy to replace one of the two continuity equations for each element respectively. But as one aim of this model is to *determine* the total flux for every element, the full system is solved, while no absolute number of the flux is given as a boundary condition (see Sect. 3.5).

For the complete model the ionization equations (7), one for each element, and the energy equations (17), (18) have to be solved together with the continuity and momentum equations (21) or (22). This means that in the case of a pure hydrogen gas seven first order differential equations have to be solved. In the case of a hydrogen-helium mixture this number is twelve.

As this system has the explicit form (16), numerical standard routines to solve a system of ordinary differential equations can be applied. In the present case the routine `D02RAF` from the NAG-library was used. This routine allows the supply of an approximate first-guess solution, automatic addition of grid points and a flexible formulation of the boundary conditions. To solve the differential equations it uses a deferred correction technique and a Newton iteration.

3.5. Boundary conditions

To solve the above mentioned first order differential equations, in the case of a pure hydrogen gas seven, or for a hydrogen-helium mixture twelve boundary conditions are needed. These are chosen from a physical point of view.

The lower boundary of the considered chromospheric layer is placed at about 8000 K, well above the temperature minimum.

Here the particle density is assumed to be of the order of some $10^{16}\,\mathrm{m}^{-3}$. This value is the often used, e.g. in Vernazza et al. (1981). The abundance of helium at the bottom is assumed to be the same as in the photosphere; this value is known quite exactly (e.g. Anders & Grevesse, 1989). The degree of ionization at the bottom is calculated from the Saha equilibrium.

At least the ionized and the neutral component of every element should enter the layer from below with the same velocity, which is due to their tight "collisional" coupling in the form of charge exchange or ionization-recombination balance. Please note, that this does not mean that the different elements must have the same velocity. There can (but does not have to) be diffusion at the bottom of the chromosphere.

The upper boundary of the layer is placed about 1000 km above the bottom. The numerical calculations have shown that for a thicker layer the results remain unchanged.

At the top the ionization rate is fixed. This means that the photon flux is given at the top. Here the flux values calculated by von Steiger & Geiss (1989) from a solar spectrum are used.

The relative velocity of the neutral and ionized component, e.g. $u_\mathrm{H}/u_\mathrm{p}$, is assumed to be constant at the top. This was used instead of the stronger condition of equal velocities, e.g. $u_\mathrm{H} = u_\mathrm{p}$, because of numerical reasons: in the case of a bad first-guess solution the solving routine was much more stable when using the weaker condition. But in the end the numerical solution results in invariably equal velocities at the top, e.g. $u_\mathrm{H}/u_\mathrm{p} = 1$ (see Fig. 3).

Table 2. Boundary conditions used for the hydrogen-helium mixture. The conditions marked with an asterisk, *, are not needed for a pure hydrogen gas. In the calculations the given values are used, unless stated otherwise.

top:	ionization rate	$\gamma_{\mathrm{H\,p}} = 0.014\,\mathrm{s}^{-1}$	
		$\gamma_{\mathrm{He\,He^+}} = 0.0044\,\mathrm{s}^{-1}$	*
	relative velocity	$(u_\mathrm{H}/u_\mathrm{p})' = 0$	
		$(u_\mathrm{He}/u_\mathrm{He^+})' = 0$	*
	heat flux	$q \approx 0.01\,\mathrm{W/m^2}$	
bottom:	temperature	$T = 8000\,\mathrm{K}$	
	total density	$N_\mathrm{H} = 8{\cdot}10^{16}\,\mathrm{m}^{-3}$	
	helium abundance	$N_\mathrm{He}/N_\mathrm{H} = 0.1$	*
	degree of ionization	$n_\mathrm{p}/n_\mathrm{H} = 0.018$	
		$n_\mathrm{He^+}/n_\mathrm{He} = 0.00053$	*
	equal velocities	$u_\mathrm{H} = u_\mathrm{p}$	
		$u_\mathrm{He} = u_\mathrm{He^+}$	*

The heat flux at the top of the layer, where the temperature reaches about $2{\cdot}10^4$ K, is chosen according to Hansteen et al. (1993), leading to about $0.01\,\mathrm{W/m^2}$ by using (15). This value is somewhat arbitrary, as it is not well known, but only calculated in models and not measured directly. However, the numerical calculations have shown that the result does not depend on the exact value of the heat flux given at the top. If it is chosen "not correctly", this results in a boundary layer for the temperature at the top, i.e. the temperature rises or drops rapidly on the last km. For this reason the heat flux is chosen to give a smooth temperature profile at the top.

In Table 2 the boundary conditions are summarized and the respective values as used in the present paper are given.

It should be noted that no absolute value for the particle flux or the velocity is given as a boundary condition or imposed as a constant of integration. The only absolute values given as a boundary condition are densities, temperature and ionization rates. Especially no absolute values of the velocities are given. Thus the particle flux through the layer will result from the boundary conditions in terms of ionization rates on the top and densities at the bottom of the layer.

4. An analytical approximation for the hydrogen gas

Before discussing the numerical solution of the full hydrogen problem it might be instructive to deal with a simplified model allowing an analytical solution. A more detailed description of the following analytic model can be found in Peter & Marsch (1997).

First of all the temperature will be assumed to be constant, which is reasoned by the fact that the ionization layer is located above the temperature minimum in the chromospheric temperature plateau. For this no temperature equation has to be solved. As the expected typical velocities are ranging below 1 km/s, a

subsonic flow can be expected; the sound speed v of hydrogen at 10^4 K is about 10 km/s. This circumstance allows one to eliminate the advective derivative $(\boldsymbol{u}\cdot\nabla)\boldsymbol{u}$ term in (2). The scale height at 10^4 K is about $H{=}v^2/g{\approx}300$ km, which is larger than the thickness of the ionization layer (see Sect. 3.2). Thus the effects of gravity are small compared to the effects of friction and may be neglected. As a first approximation the recombination can be neglected too, because it is overwhelmed by the photoionization (compare (9) and Table 2). The ambipolar effects are weak as well, i.e. the electron pressure gradient, will be neglected. The full numerical studies confirm this statement (see Fig. 4).

With these assumptions the Eqs. (1) and (2) for hydrogen are reduced to

$$(n_{\rm H}u_{\rm H})' \;=\; -\gamma_{\rm Hp}\, n_{\rm H}, \tag{23}$$

$$v^2\, n_{\rm H}' \;=\; \nu_{\rm Hp}\, n_{\rm H}(u_{\rm p}-u_{\rm H}). \tag{24}$$

The respective equations for the protons can be replaced by the conservation of the total flux and total particle density, $\Phi_{\rm H} = \phi_{\rm H}+\phi_{\rm p}$ and $N_{\rm H} = n_{\rm H}+n_{\rm p}$.

The solution of the above equations together with (7) leads to the result for the hydrogen density given by

$$n_{\rm H} = N_{\rm H}\,\frac{\gamma_\infty}{\Phi_{\rm H}\,\overline{\sigma}}\,\frac{1}{2}\left(1-\tanh\frac{s-s_I}{2\,l_{\rm ion}}\right), \tag{25}$$

where $\overline{\sigma}$ and γ_∞ are the ionization cross section and ionization rate at the top for hydrogen as given in (8) and Table 2. Following (6) the ionization length is given by $l_{\rm ion}{=}U_{\rm H}/\gamma_\infty$ with $U_{\rm H}{=}\Phi_{\rm H}/N_{\rm H}$. The symbol s_I represents the point of inflection, which has been chosen to be the origin of the s-coordinate axis, i.e. $s_I = 0$.

The velocity turns out to be nearly constant,

$$u_{\rm H} = U_{\rm H}\left[1+\left(\frac{w_{\rm H}}{U_{\rm H}}\right)^2\frac{1}{2}\left(1+\tanh\frac{s-s_I}{2\,l_{\rm ion}}\right)\right]. \tag{26}$$

This is because the ionization-diffusion speed of hydrogen, $w_{\rm H} = v_{\rm H}\sqrt{\gamma_\infty/(\nu_{\rm Hp}N_{\rm H}/n_{\rm p})}$, is small compared to the mean flow velocity $U_{\rm H}$. Following the discussion in Sect. 2.1 the latter one is in the order of $U_{\rm H}{\approx}500$ m/s, while at a typical chromospheric density of $8{\cdot}10^{16}$ m^{-3} and $T{=}10^4$ K the ionization-diffusion speed is given by $w_{\rm H}{\approx}30$ m/s.

In Fig. 2 the height profiles for the density of the neutral hydrogen and the protons (middle panel) and of the relative velocity (left panel) are shown. For comparison also the normalized densities as following from the numerical model shown below in Fig. 3 (for $N_{\rm H}^\circ = 8{\cdot}10^{16}$ m^{-3}) are plotted in the right panel. In the more realistic numerical models the density profiles are not symmetric. The main reason for this is the gravitational stratification, which was neglected in the analytical model. Because the (total) density drops exponentially the production rate of ions changes dramatically within the ionization layer. This effect can also be found in the Chapman-layer of the earth's ionosphere (see Banks & Kockarts 1973).

The inclusion of the absorption of the ionizing radiation removes one of the biggest problems of the main gas models

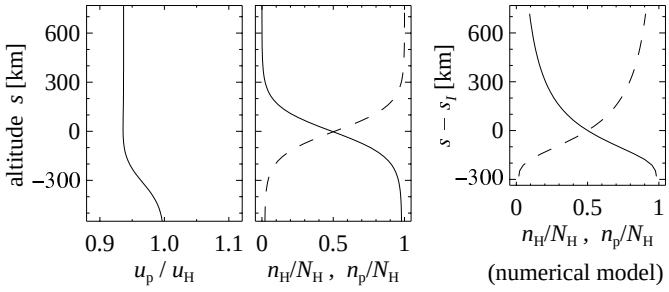

Fig. 2. Solution in the analytical H-p model and comparison with the numerical results (see text). In the middle and right panel the solid line shows the density of the neutrals, the dashed line the one of the ions.

of Marsch et al. (1995): they found that the protons leave the layer at the bottom at very high velocities. This unsatisfactory result is removed and the ions and neutrals enter the layer at the bottom with the same velocity (see Fig. 2).

While neutral and ionized hydrogen have the same velocity at the bottom, there is a diffusion at the top. This is an artifact of neglecting recombination, which causes the density of the neutrals to drop much faster in the analytical model. For this the coupling at the top is much weaker than in the numerical model which includes recombination. As it can be seen from Fig. 2, with recombination the ionization layer is more stretched out in altitude. This result shows, that in a realistic and more advanced model not only the recombination, but also the gravitational stratification has to be taken into account. As a result the thickness of the ionization layer is of the same order as the gravitational scale height in the chromosphere.

Another interesting result from this model is the determination of the total particle flux and thus the mean velocity $U_{\rm H}$. For this purpose (7) can be written in terms of the photon flux $\phi_\gamma = \gamma_{\rm Hp}/\overline{\sigma}$, i.e. $\phi_\gamma' = \overline{\sigma}\phi_\gamma n_{\rm H}$. The same can be done for the continuity equation of the protons, i.e. $\phi_{\rm p}' = \overline{\sigma}\phi_\gamma n_{\rm H}$. Applying the boundary conditions at the bottom, that all the photons are absorbed, $\phi_\gamma(-\infty) = 0$, and that the material is completely neutral, $\phi_{\rm p}(-\infty) = 0$, it follows directly, that the photon flux equals the proton flux. This especially means, that at the top (where the material is fully ionized) the total plasma flux equals the photon flux, $\Phi_{\rm H} = \Phi_\gamma$. This result can also be obtained by simply analyzing (25) in more detail. Thus also the mean velocity $U_{\rm H}$ as used in (26) can be calculated if the total density is given.

Peter & Marsch (1997) pointed out, that using the observed photon flux in the Lyman-continuum (which mainly ionizes H) to calculate the particle flux in the chromosphere, gives the observed value of the particle flux in the solar wind at the earth's orbit. However this result should be taken with a grain of salt as in their paper the recombination was neglected. In the discussion in Sect. 5.2 it becomes clear that the recombination can have a strong influence on the resulting particle flux and reduces it by a factor of 3. This consideration allows a new interpretation and simple solution of the so-called mass flux problem as stated e.g. by Leer & Holzer (1991). The solar wind particle flux is already determined by ionization processes in the so-

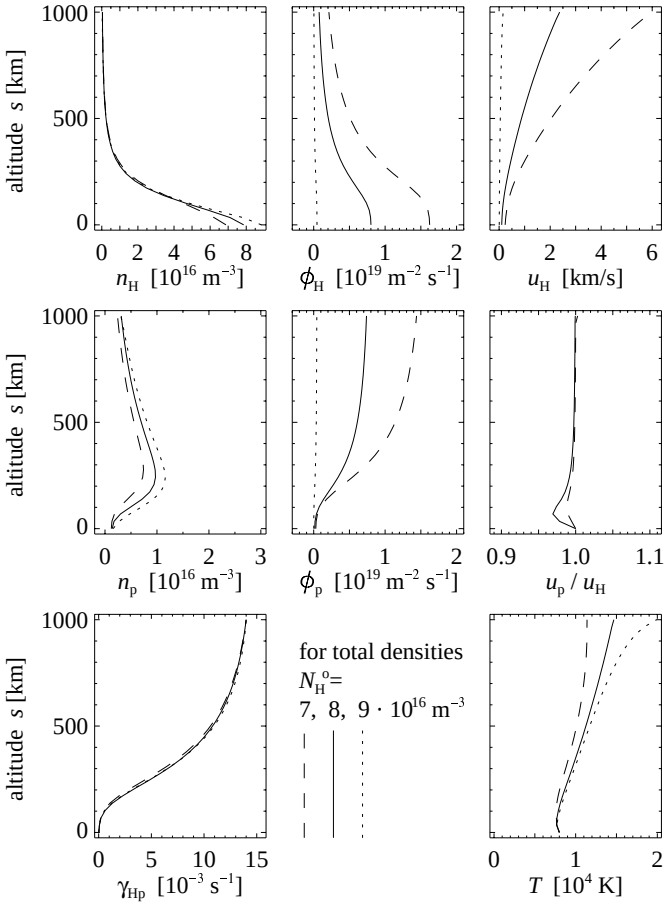

Fig. 3. Solution in a pure hydrogen gas for the densities n, the fluxes ϕ, the resulting velocities u, the ionization rate $\gamma_{\rm Hp}$ and the temperature T. The solutions are shown for three different values of the boundary condition of the total hydrogen density at the bottom, $N_{\rm H}^{\circ}$.

lar chromosphere and does not depend on the coronal plasma conditions.

5. Pure hydrogen gas: numerical studies

In this section the model results for a pure hydrogen gas will be discussed. After some more general remarks special attention will be paid to the resulting total particle flux and the mean chromospheric velocities and densities.

In Fig. 3 the solution for the densities, the particle fluxes and the velocities of neutral hydrogen and protons are shown together with the ionization rate and the temperature for three different values of the total density at the bottom, $N_{\rm H}^{\circ}$.

The most obvious result is that the velocity increases rapidly in the numerical model, while it is more or less constant in the analytical case (Fig. 3, top right panel). This is reasoned by the assumption that the flow is confined by the magnetic field structure: in the base region of a coronal funnel or a coronal loop no significant expansion is to be expected. Because of the gravitational stratification and the conservation of the total particle flux the density must increase with altitude. Because in the analytical model the gravitation is not considered, the density and thus the velocity is constant.

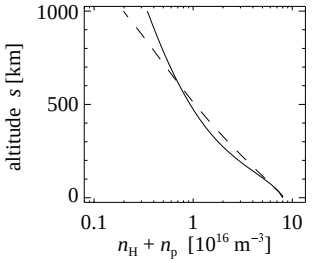

Fig. 4. Total density and ambipolar effects. This figure shows the total density in the solution for $N_{\rm H}^{\circ} = 8{\cdot}10^{16}\,{\rm m}^{-3}$ from Fig. 3 (solid line). The dashed line shows the result without ambipolar effects.

The profile of the proton density is similar to the one of the oxygen ions in the earth's ionosphere in the Chapman layer (see e. g. Banks & Kockarts, 1973). This is because the same basic processes, namely the photoionization and the gravitational stratification, are of relevance.

From Fig. 3 it can also be seen, that higher densities prevent the material from flowing. If the density is too high, a static atmosphere will be found (dotted line in Fig. 3). The behaviour of the (total) particle flux will be discussed separately in Sect. 5.2.

Normally, i. e. for densities of some $10^{16}\,{\rm m}^{-3}$, a flow of the material will be present, which can be understood as the solar wind flow in its source region. Fig. 3 (lower-right diagram) shows that this flow has a strong influence on the temperature structure. Advective transport and enthalpy flux prevent a stronger temperature gradient from building up in the lower chromosphere, even if the mean velocities are small. This leads to the conclusion that even in the chromosphere the flow of the plasma has to be considered when calculating the temperature structure.

The middle-right diagram in Fig. 3 shows that the diffusion between the neutral hydrogen and protons is weak. Only where $n_{\rm p}$ is high enough and $n_{\rm H}$ is not too small the velocities of the two components can differ significantly. But this difference is only in the order of some percent. This corresponds to the results of the analytic model of Peter & Marsch (1997), see also Sect. 4.

5.1. Total density and ambipolar effects

The total density, i. e. $N_{\rm H} = n_{\rm H} + n_{\rm p}$, decays mostly as in a barometrically stratified atmosphere, but with a small deviation (see Fig. 4).

The decline of the total density can be divided into two regions: the neutral phase with a scale height of the order of the barometrical scale height and the ionized phase, where the scale height is increased by the ambipolar effects; in the case of a single constant temperature the scale height in a pure electron-proton gas would be two times larger than in neutral hydrogen. For this the total density (solid line in Fig. 4) has a steeper gradient in the neutral phase (below ≈300 km) than in the ionized phase.

Because of this one would naively expect that the total density falls more rapidly if the ambipolar effects are neglected, i.e. the solid line in Fig. 4 should *always* be above the dashed one. But this is not the case and the question arises why the total density falls more rapidly at altitudes of about 200 – 400 km, i.e. in the region were the density of the ions and the neutrals are comparable, $n_{\rm H}{\approx}n_{\rm p}$. At that region the effects of diffusion are most important: the difference in the velocity of H and p reaches a value of about $(u_{\rm H}-u_{\rm p}){\approx}\,20$ m/s (see Fig. 3). This value is small, but as it can be seen below, the problem mentioned is caused by this (weak) diffusion:

In a simplified case of subsonic flows, constant temperature and no momentum transport due to ionization and recombination ($\gamma_{jj'}{\ll}\nu_{jk}$, see Table 1 and 2) the momentum equation (2) along the s-coordinate is given by

$$v_j^2\,n_j' \;+\; Z_j\frac{n_j}{n_{\rm e}}\,c_j^2\,n_{\rm e}' \;=\; -g-\sum_k \nu_{jk}\,n_j\,(u_j-u_k). \qquad (27)$$

Now the variation of the total density of hydrogen, $N_{\rm H}=n_{\rm H}+n_{\rm p}$ can be analyzed. If the ambipolar term $\propto c_j^2 n_{\rm e}'$ is neglected this results in the well known barometrical stratification,

$$v_{\rm H}^2\,N_{\rm H}' \;=\; -gN_{\rm H}. \qquad (28)$$

Because of the symmetry of the collisional rate the collisional term cancels out.

With the ambipolar term and assuming a single temperature, i.e. $c_j=v_j$, the above variation can be written as

$$v_{\rm H}^2\,N_{\rm H}' \;=\; -\alpha\,gN_{\rm H}, \qquad (29)$$

with the factor α given by

$$\alpha \;=\; 1\;+\;\frac{1}{2}\,\frac{\nu_{\rm Hp}}{g}\,\frac{n_{\rm H}}{N_{\rm H}}\,(u_{\rm H}-u_{\rm p})\;-\;\frac{1}{2}\,\frac{n_{\rm p}}{N_{\rm H}}. \qquad (30)$$

At the region where $n_{\rm H}{=}n_{\rm p}{=}1/2\,N_{\rm H}$ this value can be estimated as follows: at typical densities of $N_{\rm H}=10^{16}\,{\rm m}^{-3}$ the collisional rate is of the order of $\nu_{\rm Hp}=60\,{\rm s}^{-1}$ (see Table 1). With $g=274\,{\rm m/s}^2$ and the diffusion velocity $(u_{\rm H}-u_{\rm p})=20$ m/s as mentioned above this results in the factor $\alpha=1.8$.

Thus comparing the cases without and with ambipolar effects (28) and (29), in the region with a noticeable diffusion the density falls stronger if considering the ambipolar effects, as it can be seen in Fig. 4. This effect is really caused by the diffusion: if one assumes $u_{\rm H}{=}u_{\rm p}$ for a moment, it is immediately clear from (30) that in this case everywhere $\alpha{\le}1$. Thus with the help of the diffusion, resulting in $\alpha{>}1$, the problem mentioned above can be resolved.

5.2. Total particle flux

From Fig. 3 it can easily be deduced that different total particle fluxes,$\Phi_{\rm H}=\phi_{\rm H}+\phi_{\rm p}$, result for different boundary conditions for the total density at the bottom. For higher chromospheric densities near $10^{17}\,{\rm m}^{-3}$ a nearly static atmosphere is obtained, while in general a weak flow through the chromosphere will set in. As mentioned above this flow can be interpreted as the nascent solar wind. The increase of the velocity in the chromosphere is caused in this model mainly by the geometry: the flow tube, e.g. the bottom region of a coronal funnel (see Sect. 2.1), is constricted by the magnetic field and thus has a constant diameter. Because of the gravitational stratification the density drops and together with the conservation of flux this leads to the increase of the velocity with altitude.

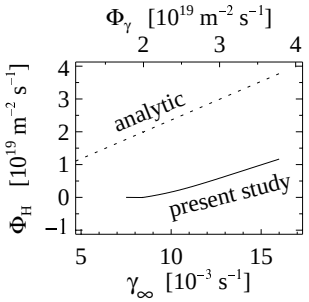

Fig. 5. Resulting total flux $\Phi_{\rm H}$ for models with different ionization rates γ_∞ at the top of the considered chromospheric layer. The dotted line indicates the result of the analytical study of Peter & Marsch (1997).

But the resulting particle flux depends also on the choice of the boundary condition of the ionization rate at the top, i.e. the photon flux, which is related to the ionization rate by $\gamma_\infty=\overline{\sigma}\Phi_\gamma$. In Fig. 5 this dependence is shown together with the one as following from the analytic model of Peter & Marsch (1997), see also Sect. 4. The present numerical study confirms the qualitative behaviour as determined by the analytical model, but the value of the particle flux at an ionization rate $\gamma_\infty=0.014\,{\rm s}^{-1}$ (von Steiger & Geiss 1989) is about a factor of three lower than in the analytical approximation. The main reason for this difference is the inclusion of recombination in the numerical model.

The numerical curve in Fig. 5 also implies that γ_∞ must exceed some threshold value to result in a non null total hydrogen flux. If the UV radiation is below this threshold, a static atmosphere will be established.

The main conclusion from Sect. 4, that the mass flux of the solar wind is determined already deep in the solar atmosphere, is confirmed by the more complete numerical model. The next step towards physical sophistication would be to include the radiative transport for the hydrogen atom as well.

5.3. Typical chromospheric velocities

The fractionation model of Peter (1996) includes the velocity of the main gas in the mechanisms leading to the FIP-effect, namely photoionization and diffusion. The main result is that the higher the velocity is, the shorter is the transit-time through the ionization-diffusion layer, and the shorter the time for the fractionation processes to act and thus the smaller is the fractionation. In his model gravity was neglected and thus the velocity through the layer was constant, as it is in the analytical approximation in Sect. 4 of this paper. Contrary to this, in the present numerical study the velocity is increasing because of the gravitational stratification (see above).

To compare the results of fractionation models based on the main gas models of the present paper (Peter 1998) with the results of Peter (1996) a typical velocity in the ionization layer has to be defined. In the recent fractionation models, like those of von Steiger & Geiss (1989), Marsch et al. (1995) or Peter (1996) the FIP-effect is driven by an ion-neutral-separation process. Thus the region of relevance is located where the ions and the neutrals of the main gas have a comparable density. This is the region around the maximum of the proton density, where the neutral density is not too low and comparable to the one of the protons. At lower altitudes, where the neutral density is much larger, the proton density is too low, at higher altitudes the situation is the other way round.

Because of this situation the (mean) velocity of the main gas at the maximum of the proton density is used to characterize the different main gas models, which can serve as a background for fractionation models. In the low-density model shown in Fig. 3 for a density of $N_{\rm H}^{\circ} = 7{\cdot}10^{16}\,{\rm m}^{-3}$ the typical velocity results in approximately 890 m/s, in the mid- and high-density case ($N_{\rm H}^{\circ} = 8$ and $9{\cdot}10^{16}\,{\rm m}^{-3}$) the velocities are in the order of 350 m/s and 20 m/s respectively.

6. Inclusion of helium

In the photosphere helium has an abundance of ca. 10%. Since its atomic weight is four times higher than that of hydrogen, helium contributes about one fourth to the total momentum transport. Therefore in contrast to the other much less abundant trace gases (together less than 1%), in the case of helium one has to examine if it has an influence on the dynamic behaviour of the bulk of material of the solar atmosphere.

The first and most obvious effect of the inclusion of helium is shown in Fig. 7 (left and middle panel). If He is included as a main gas component, i.e. with full interaction as described in (22), the density gradient is larger than in the case in which He is treated as a trace gas, i.e. when there is no reaction of helium on hydrogen. In the main gas case simply the mean molecular weight is higher, leading to a steeper decline in overall density.

But besides this, no strong changes in the dynamic behaviour can be found. This is not surprising, because the considered layer is thin, and thus the main difference between H and He, which is in the masses, is not that important. On larger scales there are stronger mass dependent effects effects, as the coronal and solar wind models e.g. of Hansteen & Leer (1995) or recently of Hansteen et al. (1997) show.

But even if there is no strong reaction on the hydrogen, it is interesting to look at the diffusion velocities and the variation of the relative abundance of helium in that thin chromospheric layer.

6.1. Diffusion

Because of the very effective Coulomb-collisions (see Table 1) the velocities of the ionized hydrogen and helium are equal throughout the layer. Only at the bottom, where the material is nearly neutral, and thus the ion collision frequency is low, a difference can occur, but because of the low ion densities there this is not of significance (see Fig. 6, middle panel).

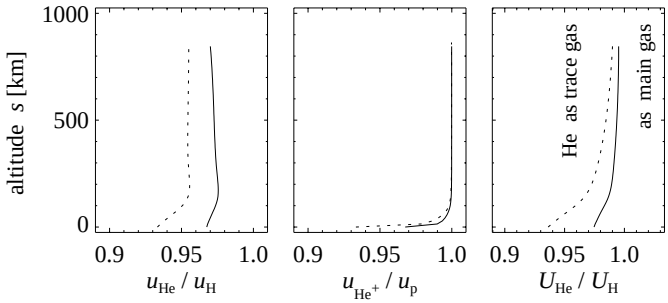

Fig. 6. Diffusion in a hydrogen-helium mixture for the model with $N_{\rm H}^{\circ}$=$8{\cdot}10^{16}\,{\rm m}^{-3}$ as shown in Fig. 3. At the top of the considered layer the elements have the same velocity, but at the bottom a significant diffusion can occur. This diffusion is stronger if helium is considered as a trace gas (dotted line).

For the neutrals the situation is quite different (Fig. 6, left panel): as the neutral-neutral collision frequency is rather small (a factor ≈1000 smaller than the ion-ion rate, again see Table 1), a velocity-difference between the neutral components can establish itself. In the present case this relative differential speed is only in the range of some percent, but finite throughout the whole layer. Additionally, with increasing height the diffusion between the neutrals get stronger. Because of their weak coupling, the heavier helium is more influenced by the gravitational force and thus stays behind the lighter hydrogen: a gravitational settlement is setting in.

In summary, the overall picture of the diffusion between the elements (neutral and ionized) is the following (see Fig. 6, right panel). A significant diffusion can occur only in the neutral phase, i.e. at the bottom of the ionization layer. There the mean (hydrogen) speed is in the order of (some) 100 m/s, while the helium diffuses with a velocity of below 10 m/s. Thus the absolute value of the diffusion velocity is small, but not vanishing. But at the top, in the ionized phase, no diffusion occurs due to the effective Coulomb-coupling.

6.2. Abundance and fractionation

The conservation of the total particle flux of every element directly couples the diffusion to the abundance variation. In Fig. 7 in the right panel the change of the He/H abundance is shown. As the diffusion is small, also the change in the abundance has to be weak. A weak depletion can be found, but the fractionation of helium to hydrogen is at least only in the order of fractions of a percent.

This clearly shows, that the abundance of helium as observed in the solar wind, (4% in the fast, 2.5% in the slow wind, Schwenn 1990) cannot be explained within the present model. An ionization-diffusion model is able to describe the fractionation of the minor species, i.e. the FIP-effect (see e.g. Peter 1998), but *fails* for an explanation of the behaviour of helium. The reason for this might be the fact that the minor species are just trapped in the solar wind, once they are ionized, i.e. from

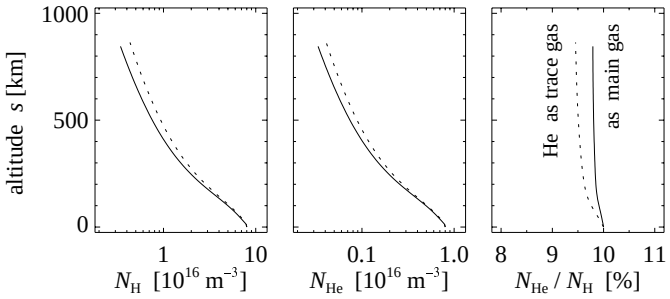

Fig. 7. Total densities and fractionation in a hydrogen-helium mixture for the model with $N_H^\circ = 8 \cdot 10^{16}$ m^{-3} as shown in Fig. 3. The total densities drop more or less barometrically and nearly no fractionation occurs. If helium is considered as a trace gas the decrease in density is less rapid and the fractionation is stronger (dotted lines).

the chromosphere on. Because of the effective Coulomb-coupling there is no possibility for diffusion and thus no additional fractionation throughout the corona and the solar wind.

The situation is different for helium. Because of its high contribution to the momentum transport (≈25%, see above) it can have a significant influence on the dynamic behaviour of the whole main gas and strong diffusion can occur e. g. by thermal forces in the transition region. These effects are described in detail in a recent paper of Hansteen et al. (1997).

The main result of this subsection is that the ionization-diffusion processes leading to the fractionation, i. e. the FIP-effect, of the minor species cannot work similarly in the case of helium.

6.3. Helium abundance and origin of CMEs

Also the strong enrichments of helium of up to 40% in the driver gas of coronal mass ejections (CMEs), see e. g. Borrini et al. (1982) cannot be explained using ionization-diffusion models for the chromosphere. Especially the speculations of Marsch et al. (1995) about an inversion layer, i. e. and enrichment of helium *in* the ionization-diffusion layer and its possible responsibility for the observed helium enrichments in the driver gas are doubtful. In the presented more sophisticated models, including also recombination, these inversion layers do not occur.

Furthermore, these models suggest that the driver gas of a CME cannot come directly, i. e. unchanged, from the deep layers of the solar atmosphere, because there helium still has its photospheric abundance of about 10%. There are two possibilities: the material comes from the chromosphere and gets fractionated within the dynamic processes of the acceleration of the CME, or, what sounds more reasonable, the driver gas originates from the corona: solar wind models like the one of Bürgi (1992) or Hansteen et al. (1997) give a strong enrichment of helium in the region around the coronal temperature maximum.

Because of this the coronal mass ejection should in deed be called “coronal” and not “solar”.

7. Summary

Multi-fluid models for a hydrogen and a hydrogen-helium ionization-diffusion layer were presented. The continuity and the momentum equations for the respective components were solved together with an energy equation. As the main aim was to supply a background gas model for minor ion fractionation models, and as these are working in the source region of the solar wind, where the mass flux originates, the main emphasis was on a detailed description of the flows.

The hydrogen model enables the determination of the plasma flux in the chromosphere. This numerical study corrects the simple analytical model of Peter & Marsch (1997), who found that the plasma flux is more or less given by the photon flux in the UV, or more precisely in the Lyman-continuum. The inclusion of the recombination reduces the resulting particle flux by a factor of three. The hydrogen model also shows that even if the velocities are small, i. e. below 1 km/s, this slow flow can have a strong influence on the temperature stratification due to the advective transport and flux of enthalpy.

The inclusion of helium gave the (negative) result that the observed depletion in the “quiet” solar wind as well as the strong enrichments in the driver gas of CMEs cannot be understood as being caused by the same process leading to fractionation of the minor species, namely the ion-neutral separation. For the minor elements the fractionation processes are located in an ionization-diffusion layer in the chromosphere (Marsch et al. 1995, Peter 1996). But in the case of helium no significant change of its abundance can be found in such a thin layer. The conclusion from this is that the abundance variation must be explained by a large-scale coronal/solar wind model, like the one of Hansteen et al. (1997).

To avoid the complexity and perhaps difficult numerical problems arising if one would combine radiative transport with plasma dynamics, we did not deal explicitly with radiative transfer in the present model. The justification for this is not well founded but rather practical: as the source region of the wind was to be described, the emphasis has been on the flows. The inclusion of radiative transport would result in a (slightly) different variation of the ionization rate with the altitude, but nevertheless the main results and conclusions should be left unchanged.

References

Anders E., Grevesse N., 1989, Geochim. Geocosm. Acta 53, 197
Athay R.G., 1981, ApJ 249, 340
Barnes A., Gazis P.R., Phillips J.L., 1995, Geophys. Res. Letters 22, (23)3309
Banks P.M., 1966, Planet. Space Sci. 14, 1105
Banks P.M., Kockarts G., 1973, Aeronomy, Part B, Academic Press
Borrini G., Gosling J.T., Bame S.J., Feldman W.C., 1982, J. Geophys. Res. 87(A9), 7370
Bürgi A., 1992, J. Geophys. Res. 97(A3), 3137
Burgers J.M., 1969, Flow equations for composite gases. Academic Press
Dowdy J.F. Jr., Rabin D., Moore R.L., 1986, Solar Physics 105, 35
Fontenla J.M., Avrett E.H., Loeser R., 1990, ApJ 355, 700
Gingerich O., de Jager C., 1968, Solar Physics 3, 5

Geiss J., 1982, Space Sci. Rev. 33, 201
Geiss J., Bürgi A., 1986, A&A 159, 1
Hansteen V.H., Leer E., 1995, J. Geophys. Res. 100(A11), 21577
Hansteen V.H., Holzer T.E., Leer E., 1993, ApJ 402, 334
Hansteen V.H., Holzer T.E., Leer E., 1997, ApJ 482, 498
Hénoux J.-C., 1995, Adv. Space Res. 15, (7)23
Hénoux J.-C., Somov B.V., 1992, First Ionization Potential Fractionation. In: Coronal Streamers, Coronal Loops and Coronal and Solar Wind Composition. ESA SP-348, p. 325
Hirshberg J., Alksne A., Colburn D.S., Bame S.J., Hundhausen A.J., 1970, J. Geophys. Res. 75, 1
Kopp R.A., Holzer T.E., 1976, Solar Phys. 49, 43
Kuin N.P.M., Poland A.I., 1991, ApJ 370, 763
Leer E., Holzer T.E., 1991, Ann. Geophysicae 9, 196
Lotz W., 1967, ApJS 14, 207
Marsch E., von Steiger R., Bochsler P., 1995, A&A 301, 261
Meyer J.-P., 1996, Abundance Anomalies in the Solar Outer Atmosphere. In: Trân Thanh Vân J., Celnikier L., Trung H.C., Vauclair S. (eds.) The Sun and Beyond. Editions Frontières, Gif-sur-Yvette, p. 27
Peres G., Rosner R., Serio S., Vaiana G.S., 1982, ApJ 252, 791
Peter H., 1996, A&A, 312 L37
Peter H., 1998, A&A submitted
Peter H., Marsch E., 1997, In: Proceedings of the Fifth SOHO Workshop, ESA SP-404, p. 591
Priest E.R., 1982, Solar Magnetohydrodynamics, D. Reidel
Rosner R., Tucker W.H., Vaiana G.S., 1978, ApJ 220, 643
Schunk R.W., 1975, Planet. Space Sci. 23, 437
Schwenn R., 1990, Large-Scale Structure of the Interplanetary Medium. In: Schwenn R., Marsch E. (eds.) Physics of the Inner Heliosphere, Springer-Verlag, Berlin, Vol. 1, p. 99
Sheeley N.R. Jr., Wang Y.-M., Hawley S.H., et al., 1997, ApJ 484, 472
von Steiger R., Geiss J., 1989, A&A 225, 222
von Steiger R., Wimmer Schweingruber R.F., Geiss J., Gloeckler G., 1995, Adv. Space Res. 15, (7)3
Ulmschneider P., Kalkofen W., 1977, A&A 57,199
Vernazza J.E., Avrett E.H., Loeser R., 1981, ApJS 45, 635
Widing K.G., Feldman U., 1992, ApJ 453, 987